Title
Microrheological modeling of lithium ion battery anode slurry

Authors
Ma, Fuduo
Fu, Yanbao
Battaglia, Vince
et al.

Publication Date
2019-10-01

DOI
10.1016/j.jpowsour.2019.226994

Peer reviewed

Microrheological Modeling of Lithium Ion Battery Anode Slurry

Fuduo Ma[1], Yanbao Fu[1], Vince Battaglia[1] and Ravi Prasher[1,2]

[1]Energy Storage and Distributed Resources Division, Lawrence Berkeley National Laboratory, Berkeley, California 94720, United States

[2]Department of Mechanical Engineering, University of California, Berkeley, California 94720, United States

* E-mail: rsprasher@lbl.gov

Abstract

The rheological properties of electrode slurries used in the manufacturing of lithium-ion batteries affect the manufacturing processes as well as the battery quality, such as electrochemical, and durability performance. There is thus an urgent need to develop a physics-based model to describe the rheological properties of these electrode slurries to enable further optimization of battery manufacturing processes. In this paper, we present a microrheological model for calculating the viscosity of electrode slurries that incorporates colloidal forces such as van der Waals and polymeric steric repulsion forces. The model shows good agreement with the experimentally determined viscosities of graphite-based anodes and can be further extended to describe the rheological properties of cathode slurries.

Introduction

The most dominant method used in the manufacture of lithium-ion batteries is the roll-to-roll (R2R) process. The R2R process typically consists of four steps: mixing of various materials including the active battery material to make the battery slurry, coating of the slurry on a current collector, drying, and calendering. The current strategy used to optimize lithium-ion battery manufacturing mainly relies on extensive trial-and-error-based experiments, which are both time

and energy consuming.[1,2] Moreover, the entire tedious process must be repeated when new electrode materials are discovered. A more fundamental understanding of the lithium-ion battery manufacturing process is highly desirable not only to facilitate battery processing but also to maximize the capacity of current electrode materials through appropriate processing. A better understanding of the 3D assembly structures of the particles within an electrode can be used to predict the end-use performance of a battery.[3-11] Although advanced microscopy techniques can be used to investigate the 3D structures of battery electrodes,[12-14] the process is slow and restricted to certain materials and the techniques are rarely used at manufacturing sites. Because mixing is the first step in making the electrode slurry, it plays a critical role in all the subsequent steps and in the final performance of the battery electrodes. Evaluation of the rheological properties provides a powerful and feasible method to determine the assembly structures of a slurry based on different mixing conditions.[15-17] In addition, rheometers have become standard test instruments at lithium-ion battery manufacturing sites.

A typical electrode slurry is composed of the active material, carbon black additive, and a polymer binder. The active material particles store lithium ions, and their content is preferentially maximized in the formulation of the electrode slurry. Carbon black additives are highly conductive and are essential for electron transport within the battery electrode. A percolated structure of carbon black particles is desired, as such a structure not only enhances the electrode conductivity but also strengthens the cohesion of electrode particles within the electrode. The polymer is added to bind the active material with the carbon black particles and adhere them onto the current collector.[18,19] As the particles typically range from several hundred nanometers to tens of micrometers in size, the electrode slurry falls in the colloidal regime in which interparticle colloidal interactions[20,21] determine the assembly behaviors of the particles and the rheological properties of the electrode slurry.

A few studies on the rheological properties of carbon black slurries for flow batteries have shown that the colloidal forces between the carbon black particles dominate the rheological and electrical performance[15,22,23]. These studies revealed that colloidal forces lead to particle aggregation, resulting in the formation of clusters. Narayanan et al.[22] introduced an aggregation-based model to describe the rheological properties of carbon black slurries; however, the model required simultaneous measurement of the electrical properties to extract various parameters

needed to model the rheological properties. Their model also did not consider the effect of the active particles, such as graphite, or the effect of the molecular weight of the polymer on the rheological properties.

In this work, we propose a very detailed physics-based microrheological model for the prediction of the rheological properties of lithium-ion battery anode slurries. The microrheological model considers the contributions from both interparticle colloidal interactions (van der Waals attraction, polymer steric repulsion, and electrostatic repulsion) and hydrodynamic interaction.[20,21] This model is further developed for multiparticle systems by mixing carbon black and graphite particles together. As the anode slurry is very complex in nature because of the presence of various materials of various sizes, the model is validated at various levels of complexity:

1) First, the rheology of the carbon black and polymer binder suspension is studied. The volume fraction of carbon black is systematically varied, and the viscosities of the various slurries are compared with those determined using the microrheological model. The interparticle attractions between carbon black particles increase with increasing carbon black to polymer binder ratios, and thus, the viscosity of the suspensions increases.
2) For the second level of complexity, the effect of the polymer molecular weight is modeled, and the modeling results are compared with experimental results.
3) Finally, graphite particles are added to the carbon black and polymer mixture. Only the hydrodynamic contribution of graphite particles to the viscosity is considered, as the graphite particles are greater than 10 μm in size such big that colloidal interactions are not important.

Experimental section

Materials

The anode active material (graphite) was supplied by Hitachi (SMG-HP1-10), the carbon black conductive additive was supplied by Imerys (Timcal C-Nergy Super C45), the KF series polyvinylidene fluoride (PVDF) polymer binders were supplied by Kureha Corporation (KF1100, KF1700, and KF9300), and the solvent N-methyl-2-pyrrolidone (NMP) was supplied by Sigma-Aldrich. Both supplier data sheet and optical microscopy show the graphite particles are large and above 10 μm. The sizes and surface charges of the carbon black particles in the NMP and PVDF

suspensions were measured using a dynamic light scattering (DLS) zeta potential meter (NanoPlus, Micromeritics). The surface charges of graphite particles were measured by the same zeta potential meter. The carbon black particle diameters were 553 nm. The zeta potentials for graphite and carbon black were −5 mV and −10 mV, respectively. The molecular weights of the KF series PVDF polymer binders were taken from Kureha's data sheets: $M_w(KF1100) = 2.8\times10^5$, $M_w(KF1700) = 5\times10^5$, and $M_w(KF9300) = 1\times10^6$.

Mixing of the anode slurry

Because of the high molecular weight of PVDF, the polymer solution was prepared by first dissolving PVDF into the NMP solvent with magnetic stirring overnight; the concentration of PVDF in NMP was ~5% wt. In the second step, carbon black particles were added to the pre-prepared PVDF/NMP solution, and the carbon black particles and PVDF/NMP mixture were mixed using a homogenizer at 4000 rpm for 1.5 h. The rheological properties of the well-mixed carbon black and PVDF/NMP slurries were investigated using a rheometer (DHR 2, TA Instruments). In the final step, a known amount of active material (graphite particles) was added into the carbon black/PVDF/NMP mixture and mixed with the homogenization again at 4000 rpm and 1.5 h to form the complete anode slurry. The rheological properties of the anode slurries were measured using the same rheometer.

Measurement of rheological properties

To measure the rheological properties of the slurries, the slurries were placed between a lower Peltier plate and an upper 40-mm parallel steel plate. Before each test, a high pre-shear rate of 80 s^{-1} was applied to the slurry for 5 min to erase the historic memory of the slurry. Following the pre-shear application, a stationary shear rate of 0 s^{-1} was applied for 5 min to allow the particles in the slurry to reach a steady-state structure.[24] Then, the viscosities of the slurries were tested from 0.1 to 500 s^{-1} using a step-wise increase of the shear rate.

Results and Discussion

In a weakly aggregated colloids suspension, the shear stress is composed of hydrodynamic and structural parts. The hydrodynamic part is due to hydrodynamic forces from the cores of fractal

aggregates and can be calculated by Krieger's formula.[25] The structural part is due to the forces transmitted through the particles' chains connecting neighboring aggregates into a transient network.[20] The aggregates or the chains of particles break down when the external shear stress is stronger than the attractions connecting the aggregates; the aggregates can also restore their structures under quiescent conditions due to the attractions. The formation and breakup of particles' chains is a result of the competition between external shear stress and interparticle interactions. Therefore, for weakly aggregated colloids, the structural stress needs to be calculated by applying the fractal aggregation concept, colloid interactions, and transient network theory to account for the change of particles' chains in the aggregates. The model presented in this paper includes contribution of both hydrodynamics interactions and structural part.

The Li-ion battery anode slurry consisted of active particles (graphite), conductive additive particles (carbon black), a polymer binder (PVDF), and a solvent (NMP). The major colloidal interactions include van der Waals, steric, electrostatic, hydrodynamic, and depletion interactions, as shown in Fig. 1a schematcally.[26] Figure 1b shows the magnitude of various interactions (discussed later). The colloidal interactions are critical between particles of sizes ranging from several hundred nanometers to a few micrometers. The primary carbon black particles are typically spherical, with a diameter ranging between 30 and 50 nm. In the manufacturing process, the carbon black particles are always fused into secondary large aggregates with sizes of several hundred nanometers. The carbon black secondary aggregates in the anode slurry we used were approximately 550 nm, as measured using DLS. Therefore, in the model validation, the carbon black secondary aggregates were assumed to be spherical and the diameter of the carbon black secondary aggregate was assumed to be $2a$=550 nm. For clarity and similarity, the carbon black secondary aggregates are hereafter called carbon black particles in this paper. In contrast, the graphite particle sizes measured using DLS were large (approximately 10 μm). The colloidal forces are much stronger for smaller particles (typically

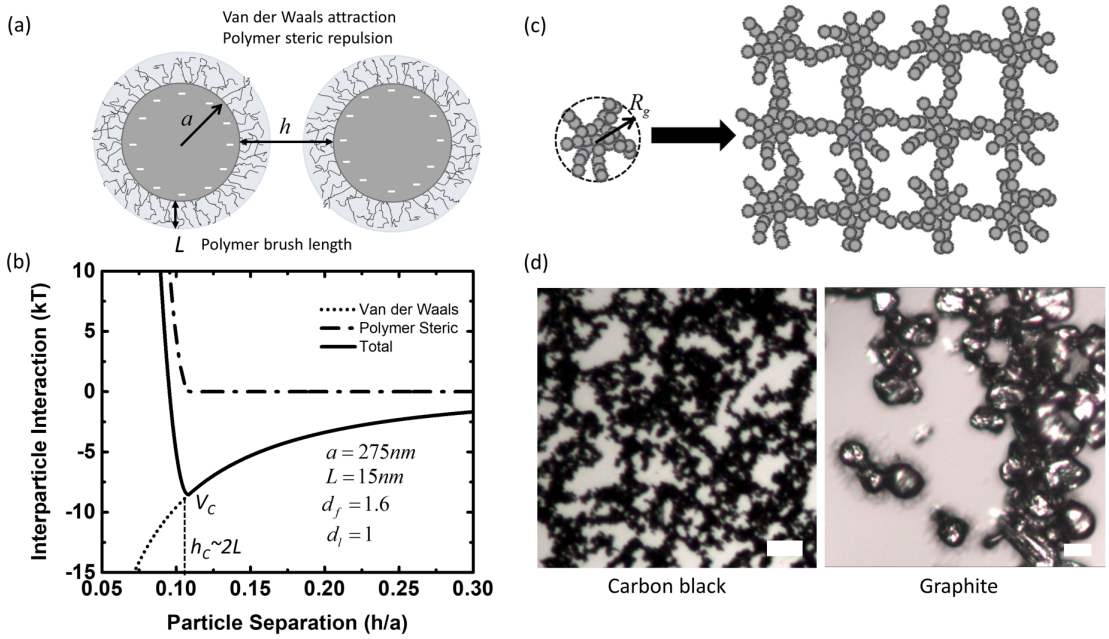

Fig. 1 Interparticle colloidal interaction and assembly behaviors of particles in anode slurry. (a) Schematic illustration of polymer-coated carbon black particles and interparticle colloidal interactions. (b) Typical interparticle potential between two carbon black particles coated with PVDF (KF1700). (c) Schematic representation of primary carbon black particles assembled into secondary aggregates with the aggregates connected into networks. (d) Optical images of assemblies of carbon black (left) and graphite (right) particles. The scale bar is 10 μm.

less then 1 μm in size). Therefore, the colloidal forces were expected to play a much larger role for the carbon black particles than for the graphite particles. It is well established in the literature that colloidal interactions can lead to the aggregation of particles[20,22]. These aggregates are fractal in nature, as observed in the schematic illustrations in Fig. 1c. The optical image in Fig. 1d shows that the carbon black particles assemble into highly branched aggregates or flocs because of the weak attractive interactions. In contrast, the graphite particles, which are relatively large, do not form interconnected fractal structures such as those of the carbon black particles because the colloidal forces are not very strong for larger graphite particles, as discussed above. The rheological properties of the carbon black suspensions were dominated by discrete aggregates at low concentrations and by the continuous network at high concentrations. The aggregates were treated as fractal objects because of their self-similarity. In the fractal concept,[25] the number N of base particles of radius a contained inside a fractal aggregate with radius of gyration (Fig. 1c) R_g is

$$N = \left(\frac{R_g}{a} \right)^{df}, \tag{1}$$

where d_f is the fractal dimension. For carbon black particles, a~275nm is the radius of the carbon black secondary aggregate. The particle aggregate volume fraction ϕ_a is related to the base particle volume fraction ϕ_p as[20]

$$\phi_a = \frac{\phi_p}{\phi_{\text{int}}}, \tag{2}$$

where the internal averaged volume fraction $\phi_{\text{int}} = \left(\frac{R_g}{a} \right)^{df-3}$.

In the mixing of carbon black with PVDF and NMP, PVDF is physically absorbed to the surface of the carbon black particles, reducing the large surface tension between the carbon black particles and NMP.[6] The length of the absorbed PVDF brush L, as shown in Fig. 1a, is a complex function of the solvent properties, particle surface morphologies, particle and polymer ratios, and polymer molecular weights.[27] The absorbed PVDF layer results in strong steric interaction between particles.[28] Based on classic Derjaguin–Landau–Verwey–Overbeek (DLVO) theory with additional steric interaction,[29,30] the total potential between two particles is

$$V_{total} = V_{steric} + V_{VDW} + V_{electrostatic}. \tag{4}$$

V_{steric} is the steric repulsion from the polymer coating, V_{VDW} is the van der Waals attraction, and $V_{electrostatic}$ is the electrostatic (double layer) repulsion due to particle surface charge.[31] Because the zeta potential of carbon black particles dispersed in NMP is very low, approximately 5 mV as measured using a zeta potential meter, the electrostatic repulsion can be safely neglected. The stability of the slurry therefore mainly arises from the steric repulsion. We calculate the two major colloidal interactions as follows.

The van der Waals attraction V_{VDW} between two spherical particles is given by[32]

$$V_{VDW} = -\frac{A(h)}{6k_BT}\left[\frac{2a^2}{h(4a+h)} + \frac{2a^2}{(2a+h)^2} + \ln\frac{h(4a+h)}{(2a+h)^2}\right], \quad (5)$$

where h is the surface-to-surface distance, k_B is the Boltzmann constant, T is the temperature, and a is the particle radius. $A(h)$ is the Hamaker constant, which can be calculated using the analytical approximation presented by Russel et al.[33]:

$$A(h) = \frac{3}{4}k_BT\left(\frac{\varepsilon_{CB}-\varepsilon_{NMP}}{\varepsilon_{CB}+\varepsilon_{NMP}}\right)^2 + \frac{3}{16\sqrt{2}}h_p v_0 \frac{(n_{CB}^2-n_{NMP}^2)^2}{(n_{CB}^2+n_{NMP}^2)^{3/2}}. \quad (6)$$

$\varepsilon_{CB} = 2.78(\varepsilon_{NMP} = 32.2)$ is the permittivity of carbon black (NMP),[34] h_p is the Planck constant, $v_0 \sim 3\times10^{-15}s^{-1}$ is the primary adsorption frequency,[35,36] and $n_{CB} = 2.0(n_{NMP} = 1.47)$ is the refractive index of carbon black (NMP).

Steric repulsion originates from the interactions between adsorbing polymers and consists of two parts (osmotic and elastic): $V_{steric} = V_{osm} + V_{el}$, as shown in Eq. 7 and 8. These two parts dominate at different interparticle separations. First, as the surface distance h between two carbon black particles decreases from infinity to approximately $2L$ (where L is the adsorbed polymer brush length shown in Fig. 1a), the carbon black particles will feel strong steric repulsion V_{OSM} due to the overlapping of polymer brushes on neighboring particles resulting in a local increase in the osmotic pressure.[32] V_{osm} is given as

$$V_{osm} = 0 \qquad h > 2L \quad (7.1)$$

$$V_{osm} = \frac{4\pi a k_BT}{v_{solvent}}\phi_{poly}^2\left(\frac{1}{2}-\chi\right)\left(\mathrm{L}-\frac{h}{2}\right)^2 \qquad L \le h < 2L \quad (7.2)$$

$$V_{osm} = \frac{4\pi a k_BT}{v_{solvent}}\phi_{poly}^2\left(\frac{1}{2}-\chi\right)\mathrm{L}^2\left(\frac{h}{2L}-\frac{1}{4}-\ln\left(\frac{h}{L}\right)\right) \qquad \mathrm{h<L} \quad (7.3)$$

$\chi < 0.5$ is the Flory–Huggins factor of PVDF in NMP which was previously measured experimentally using inverse gas chromatography.[37] $\phi_{poly} = 0.05$ is the volume fraction of polymer in the coating layer. A sensitivity calculation was performed to understand the impact of

ϕ_{poly} (varied from 5 – 15%) on the maximum attraction. Calculation showed that maximum attraction is not sensitive to ϕ_{poly} in this range. Therefore, 5% is a reasonable assumption for calculation. For the NMP solvent, the density is $1.03 g/cm^3$ and the molar mass is $99.13 g/cm^3$; therefore, $v_{solvent} = 0.16\ nm$. Second, as the neighboring particles further approach each other and the surface distance decreases to $h = L$, compression of the polymer brushes results in a loss of polymer entropy and generates an additional strong elastic steric repulsion:[36]

$$V_{el} = 0 \qquad h > L \quad (8.1)$$

$$V_{el} = \frac{2\pi a k_B T}{M_w} \phi_{poly} L^2 \rho_{poly} \left(\frac{h}{L} \ln[\frac{h}{L}(\frac{3-h/L}{2})^2] - 6\ln[\frac{3-h/L}{2}] + 3(1-\frac{h}{L}) \right) \quad h \le L \quad (8.2)$$

Here, M_w is the molecular weight of the polymer ($5\times10^5 g/mol$ for KF1700 in Fig. 1b $\rho_{poly} = 1.78 g/cm^3$ is the density of polymer, and $v_{solvent}$ is the specific volume of the solvent.[32]

A typical interparticle potential is plotted in Fig. 1b, where the y-axis is the potential/$k_B T$ and the x-axis is h/a. This plot clearly illustrates that attractive van der Waals interaction dominates at larger separation and reaches a maximum absolute value (minima in the potential) V_c at approximately $h \sim 2L$, where steric repulsion starts dominating over van der Waals attraction. The interparticle separation at which the maximum interparticle potential (absolute value) V_c is observed is h_c.[20] The maximum attraction between carbon black particles is smaller than $20 k_B T$; thus, the aggregation process of particles is reversible.[25] The neighboring particles are always constrained in a position near h_c.

Potanin *et al*.[20] developed a microrheological model based on aggregation due to colloidal forces, as discussed above. We used their microrheological model to calculate the viscosity of the slurry consisting of the carbon black particles, PVDF, and NMP. In this model, the viscosity is estimated to be the sum of the structural and hydrodynamic parts:

$$\eta_r = \eta_{struct} + \eta_{hydro} \quad (9)$$

The structural contribution η_{struct} originates from interparticle colloidal interactions and dominates at low shear rates, whereas the hydrodynamic contribution η_{hydro} is attributed to the hydrodynamic cores of fractal aggregates and dominates at high shear rates. Note that η_r is the relative viscosity with respect to the polymer and NMP solution and is given by $v_{slurry}/v_{polymer+NMP}$ where ν is the viscosity.

The particle suspension is composed of fractal aggregates or flocs, which can be easily connected into a space-filling network, as illustrated in Fig. 1c and d. Stress is transmitted through the chains of particles linking neighboring aggregates in the transient network. The creation and breakup of bonds are both taken into account. The bonds are distinguished as either soft or rigid ones. Only the rigid bonds are considered to transmit stress through multiply connected backbones as contorted elastic rods. The backbone is a fraction of the colloidal chains that elastically respond to external deformations. The soft bonds have one soft junction and deform without elastic resistance; therefore, their contribution to the external shear stress is neglected. Following the above procedures, an analytical expression can be obtained for the structural contribution to the relative viscosity:[20]

$$\eta_{struct} = \frac{\alpha}{\gamma}\frac{F_c h_c}{a^3}\phi_a\left(\frac{\phi_p}{\phi_a}\right)^{(5-2d_f-d_l)(3-d_f)} \tag{10}$$

Here, α is the fraction of collisions resulting in a rigid interaggregate chain (refers to Eq. 14 in ref. 20); γ is the shear rate; $F_c = Max[-F(h)] = -F(h_{c1})$ is the maximum bonding force; h_c is the separation at the minimum interparticle potential V_c, where h_c is very close to h_{c1}; ϕ_p is the volume fraction of the base particles; ϕ_a is the fractal aggregates assembled from the base particles (calculated using Eq.2); d_f is the fractal dimension; and d_l is the chemical dimension. The details for calculating the above parameters are given in the paper by Potanin *et al*.[20] Importantly, ϕ_a is a function of shear rate and must be calculated using a break-up criterion. At a given shear rate, steady state means that dynamic equilibrium is reached between the creation and breakup of the fractal aggregates. The equilibrium sizes of the fractal aggregates are dependent on the competition between the maximum stress from shear and the maximum binding energy from interparticle attraction. By comparing the maximum stretching force applied to a semispherical portion of a

hydrodynamic core with the critical force required for breaking the bonds, the volume fraction of fractal aggregates can be determined. The maximum stretching force can be estimated from the known solution for a spherical particle under shear as[38]

$$F_{stretching} = \frac{5\pi}{2}\eta_{struct}\gamma q^2 , \tag{11}$$

and the critical breaking force is[20]

$$F_{breaking} = \frac{F_c a}{q} , \tag{12}$$

where q is the end-to-end distance of the chains within the fractal aggregates and $q \sim kR_g$; k value is on the order of 1, 0.38 is used in the modeling for best fitting; R_g is the radius of gyration of the fractal aggregates.. By equating Eq. 11 with Eq. 12, η_{struct} can be written as

$$\eta_{struct} = \frac{2F_c a}{5\pi q^3 \gamma} . \tag{13a}$$

Solving Eq. 13a together with Eq. 11, the relationship between the fractal aggregate fraction and shear rate is determined to be

$$\gamma = \frac{\frac{2F_c aA}{5\pi q^3} - \alpha B \frac{F_c h_c}{a^3}\phi_a^2 (\frac{\phi_b}{\phi_a})^{\frac{5-2d_f-d_l}{3-d_f}}}{\eta(1-\frac{\phi_a}{\phi_m})^{-2.5\phi_m}} , \tag{13b}$$

where $A = k_0^{1/2} \cdot 2^{2+d_l}$, $B = k^{d_l+1} \cdot 2^{2+d_l}$, and ϕ_m is the maximum volume fraction of densely packed spheres. k_0 is a numerical coefficient related to the critical elastic force constant $\frac{d^2U(h_c)}{d^2h}$ as $\frac{d^2U(h_c)}{d^2h} = k_0(\frac{F_c}{h_c})$, i.e., k_0 is the dimensionless steepness of the potential. Calculating the elastic force constant $\frac{d^2U(h_c)}{d^2h}$, *i.e.*, the second derivative of particle interaction, at the potential minimum is important for calculating the critical force F_C for the particle chain breaking up under external

shear stress. The aggregate volume fraction ϕ_a is numerically a function of shear rate. Fig. 2 shows the relationship between ϕ_a and the shear rate. ϕ_a decreases with increasing shear rate. At low shear rates, ϕ_a can be much higher than the volume fraction of individual base particles, as shown in Fig. 2, indicating that individual particles are intercalated to form a network that fills the entire slurry. Therefore, the interparticle interaction that leads the base particles to assemble into large aggregates contributes significantly to the viscosity.

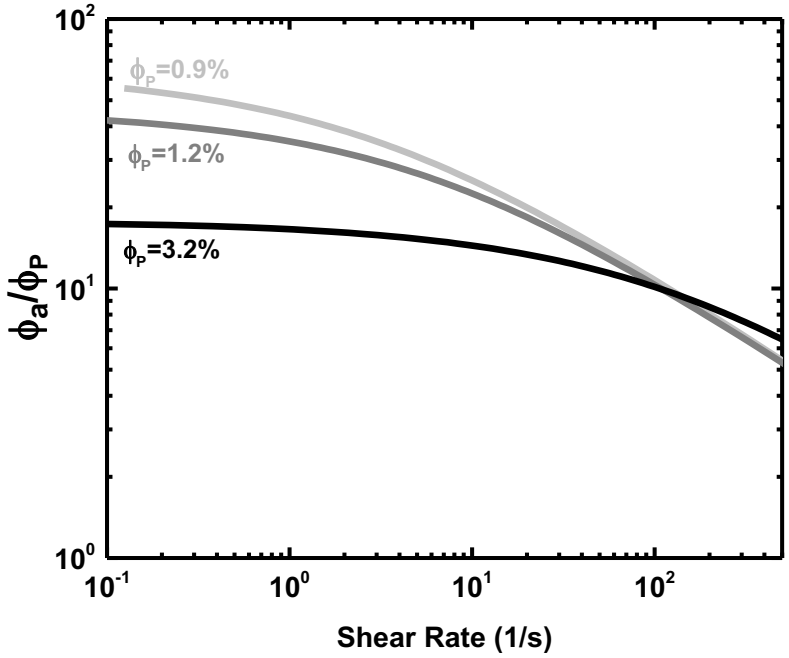

Fig. 2 Decrease of relative volume fraction of carbon black aggregates with increasing shear rate assuming $d_f = 1.6$

The hydrodynamic contribution was determined using the classic Krieger's phenomenological formula[39] but with the effective aggregate volume fraction ϕ_a:

$$\eta_{hydro} = \left(1 - \frac{\phi_a}{\phi_m}\right)^{-2.5\phi_m} . \quad (14)$$

The maximum volume fraction ϕ_m of densely packed spheres is ~ 0.61.

This microrheological model was first used to investigate the viscosity of the carbon black and polymer suspension. The particle volume fraction was systematically varied from 0.9% to

3.2%. In the mixing of the carbon black and PVDF polymer suspension, the amount of PVDF was kept constant, and the amount of carbon black was increased. Both the experimental and modeling results are presented in Fig. 3. The carbon black and polymer suspension exhibited a shear thinning behavior, with the viscosity decreasing with increasing shear rate. At low shear rates, interparticle colloidal interactions dominated and carbon black fractal aggregates interconnected into a network that fills the entire slurry. Because of the strong interparticle bonding energy and high aggregate volume fraction, the relative viscosity was high. The hydrodynamic interaction increased with increasing shear rates. For intermediate shear rates, when the hydrodynamic interaction was slightly stronger than or comparable to the maximum bonding energy between carbon black primary particles, the network and large flocs of carbon black particles disassembled into fractal aggregates. As the shear rate was further increased, the hydrodynamic interaction was enhanced and dominated over the bonding energy between base particles. The larger aggregates broke into smaller ones as well as primary particles. Therefore, the viscosity of the carbon black suspension was low and was mainly attributed to the hydrodynamic interactions of particles. The breaking and reforming of the transmit network is a reversible process for the carbon black particles with weak bonding energy. Figure 3 shows that the microrheological model generally matches well with the data. The model seems to underpredict experimental data at higher shear rates. One of the main reasons is that it is quite possible that fractals never completely break into individual particles for the shear rate available in the experiment. Another reason is that the scaling parameter k may be shear rate dependent.

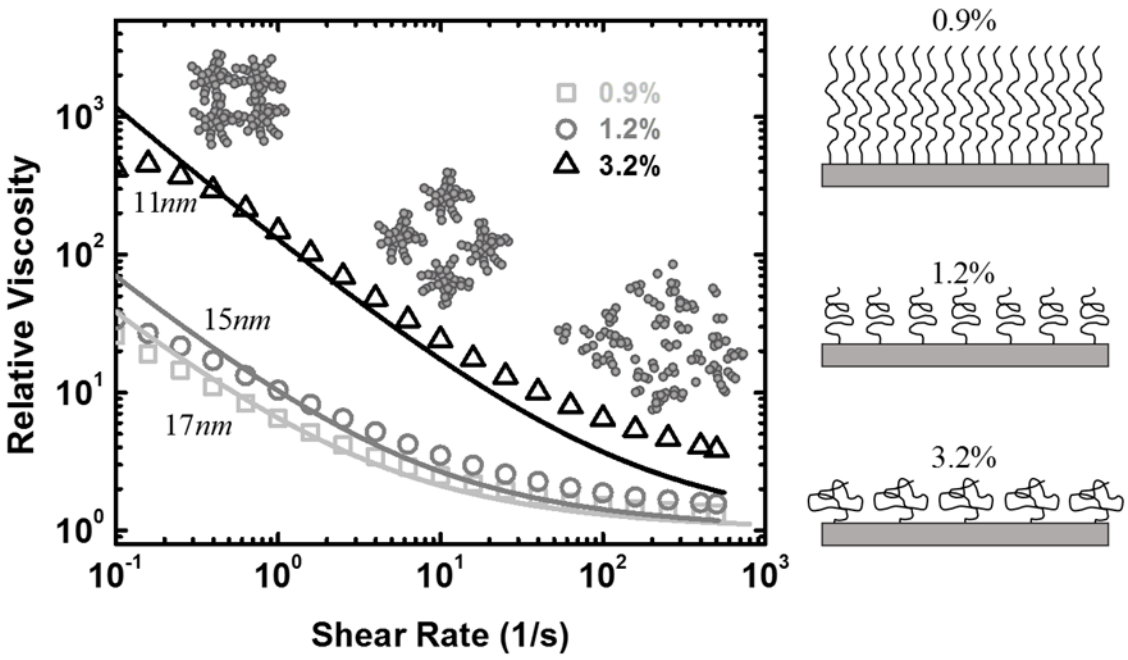

Fig. 3 Experimental and modeling results (assuming df = 1.6) for the viscosities of carbon black and PVDF (KF1700) slurries for three different particle concentrations. The light grey squares, dark circles, and black triangles are the experimental rheological data for $\varphi_P = 0.9\%, 1.2\%, \text{and } 3.2\%, respectively$, and the light grey, dark, and black lines are the modeling rheological data for $\varphi_P = 0.9\%, 1.2\%, \text{and } 3.2\%, respectively$. The schematic illustrations on the right side show the morphologies of PVDF on the carbon black surface for the three different particle volume fractions.

To obtain the best fitting, different polymer brush lengths were used in the modeling: 17, 15, and 11 nm for 0.9%, 1.2%, and 3.2% (vol%) of carbon black, respectively. The length of polymer brush is dependent on the molecular weights of the polymers. It is well known that fully adsorbed polymers curl up and that their effective length is given by the radius of gyration. The radius of gyration of an adsorbed polymer is given by[35]

$$L = \frac{l\sqrt{M_w / M_0}}{\sqrt{6}}, \tag{15}$$

where M_0 = 64.035 g/mol is the repeating subunit of PVDF, CH_2CF_2; l is the length of the subunit; and M_w is the molecular weight of PVDF. The bond lengths of C–H, C–C, and C–F are 1.09, 1.53, and 1.36 Å, respectively, and the bond angles of H–C–H and F–C–F are 109.5° and 103°, respectively. Therefore, a simple geometric calculation shows that l is ~3 Å.[40] In addition to molecular weight, the polymer brush length is also ~~sensitively~~ dependent on the volume ratios between particles and the polymer[35] because the morphologies of absorbing polymers will change

along with the available space on the particle surface. For example, when the carbon black volume fraction is high, i.e., 3.2%, there is enough space on the carbon black surface to accommodate PVDF and allow the PVDF polymer chains to hold a curl-up morphology. The PVDF polymers are in the "relaxed" structure shown in the schematic illustration in Fig. 3. The polymer brush length L (10 nm) calculated using Eq. 15 is very close to the value used for best-fit modeling. The length of polymer on carbon black particles is also dependent on the surface area of the carbon black particles. A higher concentration of carbon black particles leads to a smaller polymer length, as shown in Fig. 3. Such behaviors have been previously addressed in both theoretical and experimental works.[41-44] As discussed above, the maximum attraction between two carbon black particles is dependent on the length of the absorbed polymer brush because the very strong polymer steric repulsion starts to dominates over van der Waals attraction when the interparticle surface-to-surface distance reaches 2L. For a smaller polymer brush length, the two particles become closer, resulting in stronger interparticle attraction. Therefore, as shown in Fig. 3, the viscosity increases dramatically with a relatively small increase in the volume fraction of carbon black particles from 0.9% to 3.2%.

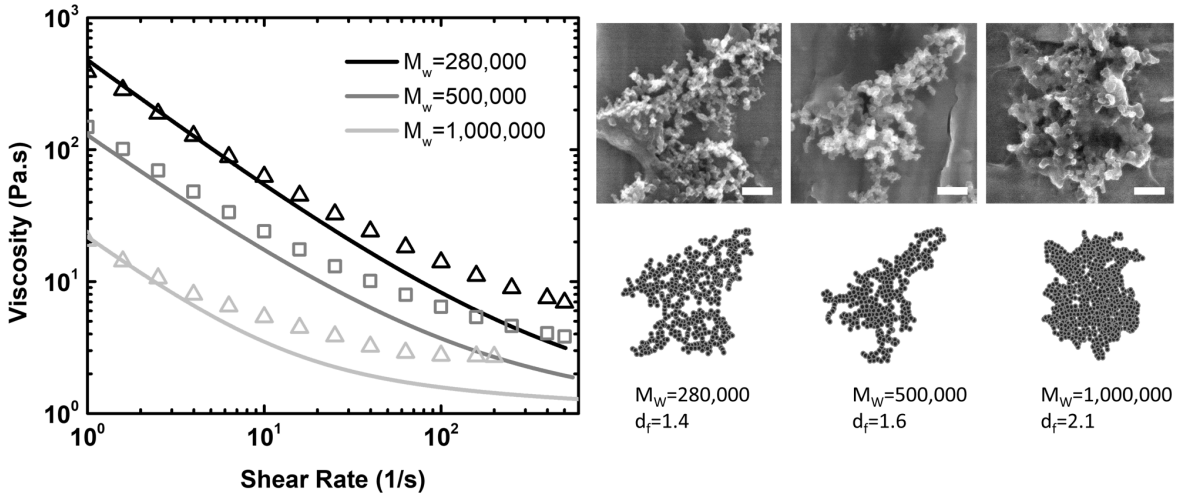

Fig. 4 Rheological properties of 3.2 vol% carbon black particles in polymer suspension with three different molecular weights: $M_w(KF1100) = 280{,}000$, $M_w(KF1700) = 500{,}000$, and $M_w(KF9300) = 1{,}000{,}000$. SEM images and schematic illustrations of carbon black fractal aggregates in different polymer solutions. The scale bar is 500 nm.

To further validate our model, we varied the molecular weight of the polymer binder (PVDF). The molecular weight is an important parameter in determining the mechanical and electrical properties of electrodes and the final battery performance.[45,46] Therefore, we evaluated

the effect of the polymer molecular weight on the aggregations and viscosity of carbon black and polymer suspensions. Three different molecular weights were used: KF1100=280,000, KF1700=500,000, and KF9300=1,000,000. As shown in Fig. 4, all three samples exhibited shear thinning behavior. The volume fraction of carbon black particles of 3.2% was selected for the molecular weight study, as the particle surface area is large enough to accommodate the polymers. The polymer brush lengths were calculated using Eq. 15: 7.5, 10, and 14.2 nm for KF1100, 1700, and 9300 PVDF, respectively. The calculated values are very close to the fitted polymer lengths in the modeling: 8, 11, and 16 nm, respectively. The decrease in the polymer brush length enhances the interparticle attraction and relative viscosity of the particle suspension. Therefore, as clearly illustrated in Fig. 4, the relative viscosity increases with decreasing polymer molecular weight. However, only changing the polymer brush length is not sufficient to obtain good fitting between the modeling and experimental data. In addition to the polymer brush length, the fractal dimension is used as a secondary fitting parameter for modeling of carbon black in polymer solutions with different molecular weights.

The fractal dimension is used to characterize the structure of an aggregation of sub-micro particles. The aggregation changes from a diffusion-limited cluster aggregation (DLCA) to a reaction-limited cluster aggregation (RLCA) with increasing fractal dimension.[47] For smaller values of fractal dimension, the aggregations have more opened structures, whereas for larger values of fractal dimension, the aggregations have more closed structures. It has been demonstrated experimentally[48-50] and by computer simulations[51-53] that the fractal dimension is a function of the interparticle forces. Lin et al.[49] observed that the transition between DLCA and RLCA aggregations for several different types of colloidal particles is a universal phenomenon. The repulsion between the colloidal particles is tuned by modifying the surface charges. When the particle surface is strongly charged, the repulsion is strong, the aggregation force is weak, and the aggregation is slower than diffusion. Thus, the particles form a RLCA aggregation. In contrast, when the surface charge is less, aggregation is more rapid than particle diffusion. Thus, the particles assemble into a DLCA aggregation. In our work, we used polymer steric interactions as a tool to change aggregations between DLCA and RLCA. Though the interactions are different, the mechanism for controlling aggregation fractal dimension is very similar.

In the carbon black and polymer slurry, the repulsion/attraction between particles is controlled mainly by the polymer steric interaction. For a low-molecular-weight polymer, the polymer brush length is smaller, the two particles are closer with stronger attraction. This phenomenon is similar to that for weakly charged particles; thus, the reaction/aggregation is more rapid than particle diffusion. The carbon black particles assemble into DLCA aggregations, the structures of which are more open. With increasing molecular weight, the polymer length increases. Particles stop at a relative further distance; thus, the attraction is weaker. This phenomenon is similar to that for strongly charged colloids. Thus, the carbon black particles assemble into RLCA aggregations. These different aggregations at different PVDF molecular weights are successfully captured in the SEM images presented in Fig. 4. As the PVDF molecular weight changes from 280,000 for KF1100 to 1,000,000 for KF9300, the carbon black aggregation changes from DLCA to RLCA. In addition, the fractal dimension d_f for the best data fitting in the modeling is 1.4, 1.6, and 2.1, for KF1100, KF1700, and KF9300, respectively. The values of d_f fall within the range of those reported in the literature.[47] The morphologies of the aggregations of carbon black particles profoundly affect the viscosity of the slurry. When the aggregation has a more opened structure, such as for DLCA aggregation, the probability for aggregations to collide and interconnect is higher than for RLCA aggregation.[54] Therefore, the carbon black particles dispersed in low-molecular-weight PVDF form more opened DLCA aggregation with a higher relative viscosity than those dispersed in PVDF suspensions with higher molecular weights.

Finally, we modeled the steady-state rheology of the entire anode slurry containing all the materials including graphite (with a diameter, on average, greater than 10 μm). As mentioned in the earlier section, colloidal interactions are only important between particles with sizes ranging from hundreds of nanometers to a few micrometers. This phenomenon was further validated by conducting experiments with only graphite and the polymer. Fig. 5 shows that for the 26 vol% of graphite, the viscosity did not show any shear thinning behavior as was the case for the carbon black particles (Fig. 3). Fig. 5 shows that Krieger's theory[39] works fairly well for the graphite and polymer solution, considering the arbitrary geometry and polydisperse size distribution of the graphite particles. Krieger's theory for graphite particle is expressed as

$$\eta_{graphite} = \left(1 - \frac{\phi_{graphite}}{\phi_m}\right)^{-2.5\phi_m} . \tag{16}$$

As observed in Eq. 14, because there is no aggregation, there is no dependence of the viscosity of graphite on the shear rate. The optical images of the pure carbon slurry and pure graphite slurry in Fig. 1d also reveal that unlike the nano-sized carbon black particles, the larger graphite particles are separate without forming an aggregating network.

In the final set of experiments, we mixed everything together (graphite, carbon black, and polymer). In this mixture of carbon black and graphite particles, the carbon black particles still formed a network, and the graphite particles were embedded within the network of carbon black particles, as shown in the schematic illustrations and SEM image of the dried anode electrode in Fig. 5.

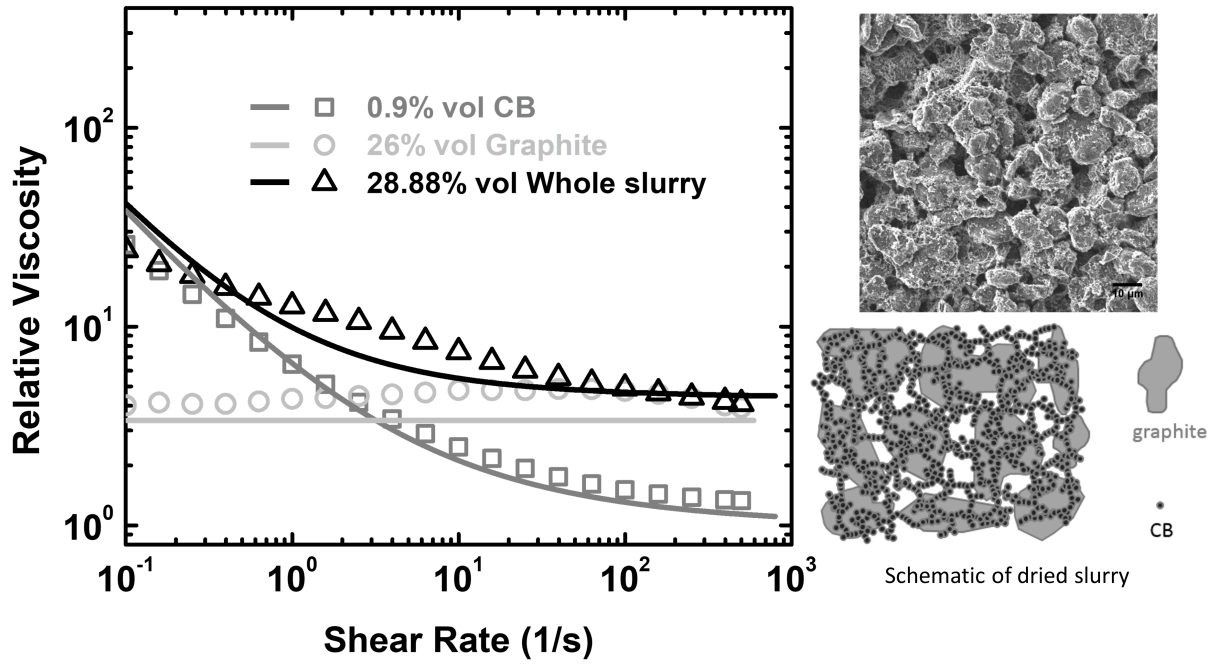

Fig. 5 The experimental (markers) and modeling (solid lines) results of the carbon black/polymer slurry, graphite/polymer slurry, and entire anode slurry are shown on the left side. An SEM image of the dried slurry is shown on the upper right side. The larger particles are graphite, and the interconnected smaller particles covering the graphite are carbon black particles. A schematic illustration of the entire dried slurry is presented below the SEM image.

For the multiparticle system, we assume that both carbon black and graphite contribute to the viscosity in series. Therefore, their individual contributions are added, and the effective relative viscosity is given by

$$\eta_r = \eta_{graphite} + \eta_{CB}\,. \tag{17}$$

Because colloidal interactions are not important for graphite, it was assumed that $\eta_{graphite}$ can be modeled using the Krieger's theory (Eq. 14). Because carbon black still forms the aggregates and network in the entire slurry, the microrheological modeling (Eq. 9) was used to interpret the carbon black data. Fig. 5 shows that the calculated viscosity given by Eq. 17 matches well with the data.

Fig. 5 shows that the viscosity of the entire anode slurry is similar to that of the carbon black and polymer solution at lower shear rates. This similarity is observed because the viscosity of the entire slurry results from the stress transmitted through the chains within the aggregated network of carbon black particles, while the hydrodynamic contribution from graphite particles is negligible. With increasing shear rates, the hydrodynamic interactions increase and graphite dominates the viscosity.

Conclusion

The viscosities of carbon black and polymer binder suspensions as well as entire anode slurries were well predicted by the microrheological model developed in this paper. The carbon black particles form an aggregate network and contribute significantly to the viscosity of the entire slurry, and both the interparticle colloidal and hydrodynamic interactions were considered in the modeling. The graphite particles are embedded within the network formed by the carbon black particles, and only hydrodynamic interaction was considered in the modeling. The interactions between carbon black particles are strongly dependent on the particle to polymer binder ratio and the molecular weight of the polymer binder. The changes in the interparticle interactions are clearly reflected in the particle assembly structures and thus the viscosity of the slurry. All these changes were successfully captured by the model. This microrheological modeling incorporating fundamental colloidal forces provides a greatly improved understanding of battery processing and can serve as a powerful tool for the optimization of battery manufacturing. The microrheological model developed in this paper can also be further extended to cathode slurries.

Acknowledgements

This work was supported by the Assistant Secretary for Energy Efficiency and Renewable Energy, Advanced Manufacturing Office, of the U.S. Department of Energy under Contract No. DEAC02-05CH11231. We are thankful to Xiangyun Song for assistance with capturing SEM images.

References

(1) Li, J. L.; Daniel, C.; Wood, D. *J Power Sources* **2011**, *196*, 2452.

(2) Wood, D. L.; Li, J. L.; Daniel, C. *J Power Sources* **2015**, *275*, 234.

(3) Bauer, W.; Notzel, D. *Ceram Int* **2014**, *40*, 4591.

(4) Bauer, W.; Notzel, D.; Wenzel, V.; Nirschl, H. *J Power Sources* **2015**, *288*, 359.

(5) Jaiser, S.; Muller, M.; Baunach, M.; Bauer, W.; Scharfer, P.; Schabel, W. *J Power Sources* **2016**, *318*, 210.

(6) Wenzel, V.; Nirschl, H.; Notzel, D. *Energy Technol-Ger* **2015**, *3*, 692.

(7) Liu, G.; Zheng, H.; Kim, S.; Deng, Y.; Minor, A. M.; Song, X.; Battaglia, V. S. *J Electrochem Soc* **2008**, *155*, A887.

(8) Ender, M.; Joos, J.; Carraro, T.; Ivers-Tiffee, E. *Electrochem Commun* **2011**, *13*, 166.

(9) Stephenson, D. E.; Walker, B. C.; Skelton, C. B.; Gorzkowski, E. P.; Rowenhorst, D. J.; Wheeler, D. R. *J Electrochem Soc* **2011**, *158*, A781.

(10) Zielke, L.; Hutzenlaub, T.; Wheeler, D. R.; Manke, I.; Arlt, T.; Paust, N.; Zengerle, R.; Thiele, S. *Advanced Energy Materials* **2014**, *4*, 1301617.

(11) Forouzan, M. M.; Mazzeo, B. A.; Wheeler, D. R. *J Electrochem Soc* **2018**, *165*, A2127.

(12) Higa, K.; Zhao, H.; Parkinson, D. Y.; Barnard, H.; Ling, M.; Liu, G.; Srinivasan, V. *J Electrochem Soc* **2017**, *164*, A380.

(13) Liu, Z.; Cronin, J. S.; Chen-Wiegart, Y. C. K.; Wilson, J. R.; Yakal-Kremski, K. J.; Wang, J.; Faber, K. T.; Barnett, S. A. *J Power Sources* **2013**, *227*, 267.

(14) Ender, M.; Joos, J.; Weber, A.; Ivers-Tiffee, E. *J Power Sources* **2014**, *269*, 912.

(15) Youssry, M.; Madec, L.; Soudan, P.; Cerbelaud, M.; Guyomard, D.; Lestriez, B. *Phys Chem Chem Phys* **2013**, *15*, 14476.

(16) Dinsmore, A. D.; Weitz, D. A. *J Phys-Condens Mat* **2002**, *14*, 7581.

(17) Silbert, L. E.; Melrose, J. R. *J Rheol* **1999**, *43*, 673.

(18) Liu, G.; Zheng, H.; Song, X.; Battaglia, V. S. *J Electrochem Soc* **2012**, *159*, A214.

(19) Zheng, H. H.; Yang, R. Z.; Liu, G.; Song, X. Y.; Battaglia, V. S. *J Phys Chem C* **2012**, *116*, 4875.

(20) Potanin, A. A.; Derooij, R.; Vandenende, D.; Mellema, J. *J Chem Phys* **1995**, *102*, 5845.

(21) Potanin, A. A.; Russel, W. B. *Phys Rev E* **1996**, *53*, 3702.

(22) Narayanan, A.; Mugele, F.; Duits, M. H. G. *Langmuir* **2017**, *33*, 1629.

(23) Richards, J. J.; Hipp, J. B.; Riley, J. K.; Wagner, N. J.; Butler, P. D. *Langmuir* **2017**, *33*, 12260.

(24) Trappe, V.; Weitz, D. A. *Physical Review Letters* **2000**, *85*, 449.

(25) Genovese, D. B. *Adv Colloid Interfac* **2012**, *171*, 1.

(26) Dixit, M. B.; Harkey, B. A.; Shen, F.; Hatzell, K. B. *J Electrochem Soc* **2018**, *165*, F264.

(27) Stuart, M. A. C. *Polym J* **1991**, *23*, 669.

(28) Bauer, W.; Nötzel, D. *Ceram Int* **2014**, *40*, 4591.

(29) Derjaguin, B.; Landau, L. *ActaPhysico chemica URSS* **1941**, 633.

(30) Verwey, E. J. W. *The Journal of Physical and Colloid Chemistry* **1947**, *51*, 631.
(31) Hanus, L. H.; Hartzler, R. U.; Wagner, N. J. *Langmuir* **2001**, *17*, 3136.
(32) Fritz, G.; Schadler, V.; Willenbacher, N.; Wagner, N. J. *Langmuir* **2002**, *18*, 6381.
(33) Russel, W. B.; Saville, D. A.; Schowalter, W. R. *Colloidal dispersions*; Cambridge University Press: Cambridge ; New York, 1989.
(34) Zhu, M.; Park, J.; Sastry, A. M. *J Electrochem Soc* **2011**, *158*, A1155.
(35) Israelachvili, J. N. *Intermolecular and surface forces*; 2nd ed.; Academic Press: London ; San Diego, 1991.
(36) Ogden, A. L.; Lewis, J. A. *Langmuir* **1996**, *12*, 3413.
(37) Okabe, M.; Wada, R.; Tazaki, M.; Homma, T. *Polym J* **2003**, *35*, 798.
(38) Goldsmith, H. L.; Mason, S. G. In *Rheology*; Eirich, F. R., Ed.; Academic Press: 1967, p 85.
(39) Krieger, I. M.; Dougherty, T. J. *Transactions of the Society of Rheology* **1959**, *3*, 137.
(40) Tonelli, A. E. *Macromolecules* **1976**, *9*, 547.
(41) Degennes, P. G. *Macromolecules* **1980**, *13*, 1069.
(42) Milner, S. T.; Witten, T. A.; Cates, M. E. *Macromolecules* **1988**, *21*, 2610.
(43) Lai, P. Y.; Halperin, A. *Macromolecules* **1991**, *24*, 4981.
(44) Moh, L. C. H.; Losego, M. D.; Braun, P. V. *Langmuir* **2011**, *27*, 3698.
(45) Yoo, M.; Frank, C. W.; Mori, S. *Chem Mater* **2003**, *15*, 850.
(46) Yoo, M.; Frank, C. W.; Mori, S.; Yamaguchi, S. *Chem Mater* **2004**, *16*, 1945.
(47) Bushell, G. C.; Yan, Y. D.; Woodfield, D.; Raper, J.; Amal, R. *Adv Colloid Interfac* **2002**, *95*, 1.
(48) Liu, J.; Shih, W. Y.; Sarikaya, M.; Aksay, I. A. *Phys Rev A* **1990**, *41*, 3206.
(49) Lin, M. Y.; Lindsay, H. M.; Weitz, D. A.; Ball, R. C.; Klein, R.; Meakin, P. *Nature* **1989**, *339*, 360.
(50) Weitz, D. A.; Huang, J. S.; Lin, M. Y.; Sung, J. *Physical Review Letters* **1985**, *54*, 1416.
(51) Meakin, P.; Wasserman, Z. R. *Phys Lett A* **1984**, *103*, 337.
(52) Hurd, A. J.; Schaefer, D. W. *Physical Review Letters* **1985**, *54*, 1043.
(53) Brown, W. D.; Ball, R. C. *J Phys a-Math Gen* **1985**, *18*, L517.
(54) Crawford, N. C.; Williams, S. K. R.; Boldridge, D.; Liberatore, M. W. *Langmuir* **2013**, *29*, 12915.